aerospace

MDPI

Article

Experimental Study of the Effect of the Initial Droplet Diameter on the Evaporation Characteristics of Unsymmetrical Dimethylhydrazine Droplets in a Subcritical Environment

Gangqiang Wu, Wansheng Nie, Congling Yang, Siyin Zhou and Hui Wang *

Department of Aerospace Science and Technology, Space Engineering University, Beijing 101416, China; gangqiangwu@yeah.net (G.W.); nws1969@126.com (W.N.); yangcongling2023@126.com (C.Y.); siyin_zhou@126.com (S.Z.)

* Correspondence: hui_wang@hgd.edu.cn

Abstract: The evaporation characteristics of unsymmetrical dimethylhydrazine droplets with different initial diameters in a subcritical environment were experimentally investigated with the temperature–pressure separation technique. The evaporation processes of unsymmetrical dimethylhydrazine droplets with different initial diameters in this environment have the same general pattern. All the studied droplets exhibit a short transient heating phase and a steady-state evaporation phase obeying d^2. Notably, the expansion of the transient heating phase gradually increases with increasing ambient pressure. The change in diameter squared $(\Delta d^2)_{max}$ increases from 1.03% at 1 MPa to 12.48% at 5 MPa. Under subcritical conditions, the evaporation rate decreases linearly with decreasing droplet diameter, and the droplet evaporation lifetime increases linearly. Changes in the initial droplet diameter may still have a large effect on droplets smaller than those studied here. When the ambient pressure is not greater than 3 MPa, the change in the steady-state evaporation time for both medium- and large-diameter droplets accounts for more than 70% of the variation in the droplet evaporation lifetime. As the ambient pressure increases to 4 MPa and 5 MPa, the percentage of the change in the transient heating time contributing to the variation in the droplet evaporation lifetime gradually increases to more than 45%.

Keywords: unsymmetrical dimethylhydrazine; initial droplet size; droplet evaporation; evaporation rate; evaporative lifetime

Citation: Wu, G.; Nie, W.; Yang, C.; Zhou, S.; Wang, H. Experimental Study of the Effect of the Initial Droplet Diameter on the Evaporation Characteristics of Unsymmetrical Dimethylhydrazine Droplets in a Subcritical Environment. *Aerospace* **2024**, *11*, 297. https://doi.org/10.3390/aerospace11040297

Academic Editor: Carmine Carmicino

Received: 26 February 2024
Revised: 2 April 2024
Accepted: 8 April 2024
Published: 11 April 2024

1. Introduction

Unsymmetrical dimethylhydrazine (UDMH) has good physical and chemical stability and can be stabilized at ambient temperature and pressure, which makes it a major power source for various types of spacecraft. In the spray combustion process of a liquid rocket motor, the dense droplets are not burned individually but are converted from the liquid phase to the gas phase by an evaporation process to feed the external diffusion flame around the droplet cloud [1,2]. The droplets formed by the spray have a wide range of size distributions and may exist in a variety of states. To gain a more comprehensive understanding of spray combustion, it is highly important to investigate the evaporation characteristics of droplets with varying initial diameters. This approach is even more important for guiding engineering application processes.

There have been many reports on liquid propellant-related single-droplet evaporation characteristics [3–8], but few studies have investigated UDMH single-droplet evaporation characteristics as well as the evaporation characteristics of different initial droplets [9–12]. Szekely and Faeth et al. [13,14] investigated the evaporation characteristics of JP-10 droplets with initial diameters ranging from 272 μm to 1350 μm at different equivalence ratios, and the results showed that the evaporation rate constant decreased with decreasing droplet diameter. Ju et al. [15] combined the UNIQUAC Functional-group Activity Coefficients

(UNIFAC) method [16] and the nonequilibrium evaporation law [17,18] to establish a multicomponent evaporation model to predict the evaporation performance of dimethyl ether (DME) droplets with different initial contents. According to the published results, the initial droplet diameter leads to a decrease in the "peak" evaporation rate of both components in the DME/n-heptane droplet. In their study, Verwey et al. [19] conducted experiments to evaluate how heptane and decane droplets of various sizes (ranging from 140 μm to 710 μm in diameter) evaporate and investigated the important role of natural convection in evaluating the evaporation mechanism of droplets. Researchers have shown that the steady-state evaporation rate is directly related to the initial diameter (d_0) under all experimental conditions. The steady-state evaporation rate was found to be a linearly increasing function of d_0 for all the experimental conditions. In their study, Dgheim et al. [20] simulated heat and mass transfer processes for three-component fuel droplets evaporating in a high-temperature medium. They demonstrated that under low Reynolds number conditions, the variation in droplet d^2 is associated with three distinct rates of evaporation. The average evaporation rate decreases as the initial droplet radius decreases. The evaporation characteristics of droplets consisting of ethanol/water and acetic acid/water, as well as individual ethanol and kerosene droplets, were investigated during depressurization through an experimental and numerical analysis by Liu et al. [21,22]. The analysis showed that the smaller the droplet diameter was, the faster the droplet evaporation rate and the lower the minimum temperature of the droplet during the pressure drop stage. Lorenzini et al. [23] numerically simulated the evaporation process of a single droplet in air using STAR-CCM and version 5.04.012 software, and the simulation results showed that the initial droplet diameter was inversely proportional to the mass evaporation of the droplet. Y. Ruan et al. [24] used a numerical simulation to study the evaporation process of liquid nitrogen droplets in a high-velocity gas stream. The numerical results show that droplets of different diameters accelerate the evaporation process with increasing gas flow rate. As the diameter increases, the rate of evaporation also increases. In their study, Stagni and his colleagues [25] examined how the initial size of droplets affected the evaporation of crude fast pyrolysis bio-oil (FPBO) and droplets consisting of a 50% volume mixture of FPBO and ethanol at atmospheric pressure. These findings demonstrated that as the diameter increases, the duration of droplet evaporation also increases. Verwey et al. [26,27] conducted experiments to examine how the initial size of droplets affects their evaporation properties in both stationary and turbulent environments. The results showed that the evaporation rate in a turbulent environment increases with the initial droplet diameter and turbulence intensity, and the evaporation lifetime decreases accordingly. The evaporation rate and normalized lifetime in the static environment do not change with the initial droplet diameter. An experimental study was carried out by Madjid Birouk et al. [28] on biodiesel droplets with initial diameters ranging from 1.00 mm to 1.50 mm. The findings revealed that the evaporation rate of these droplets is influenced by both turbulence and ambient pressure, with turbulence playing a more significant role as the ambient pressure increases.

The main shortcomings of the research on UDMH droplet evaporation characteristics are as follows: first, due to the highly toxic and corrosive nature of UDMH, there are few studies on UDMH droplet evaporation; second, the working pressure in the current research on the evaporation characteristics of UDMH is relatively low, and the maximum pressure is only 3 MPa, which is far from the actual engine's working conditions; and finally, the accurate control of droplet generation in a high-pressure environment is more difficult, resulting in difficulty in achieving consistency in the initial droplet diameter. At the same time, the size distribution of spray droplets formed by the rocket motor nozzle is wide, and there are many initial states. Therefore, the evaporation characteristics of UDMH droplets with different initial diameters under a subcritical pressure environment (1–5 MPa) are experimentally investigated in this paper based on the temperature-pressure separation technique, high-speed backlight imaging technique and copressurized droplet generation system, which is highly important for furthering studies related to the evaporation characteristics of UDMH droplets and understanding the evaporation characteristics of droplets

with different initial states. This study can also provide guidance for the engineering design and improvement of conventional liquid rocket motors using hydrazine as the main fuel.

2. Experimental Apparatus and Methods

2.1. Experimental Apparatus

Figure 1 shows a schematic diagram of the single-droplet steady-state evaporation device. The relevant technical details have also been described in detail in a previous study [29]. Droplets with different initial diameters are generated by the droplet generation system, which consists of a servomotor, a reduction mechanism, a screw, a syringe pump, and a hanging wire, where the encoder resolution of the servomotor is set to 7200 pulses/revolution, the reduction ratio of the reduction mechanism is 1:40, the pitch of the screw is 1 mm, and the inner diameter of the syringe pump is 22 mm, resulting in a volume resolution of the droplet generation system of 0.475 mm^3. First, the droplet generation system generates droplets with different diameters under a high-pressure and room-temperature environment, and then these droplets enter a high-pressure and high-temperature experimental environment, which effectively avoids the negative factors of generating droplets in the experimental environment that lead to droplet preheating in advance and affect the initial state of the droplets. Second, the volume resolution of the droplet generation system ensures the consistency of the initial droplet diameters to the maximum extent. Droplets with different initial diameters are suspended on the spherical endpoints of inverted 'J'-type metal wires. The high-temperature heating furnace used for evaporation adopts electromagnetic induction heating technology, which is driven by a cylindrical device to move from top to bottom, ensuring that the droplets are completely within the evaporation environment. High-speed backlight imaging technology is used to record the droplet evaporation process.

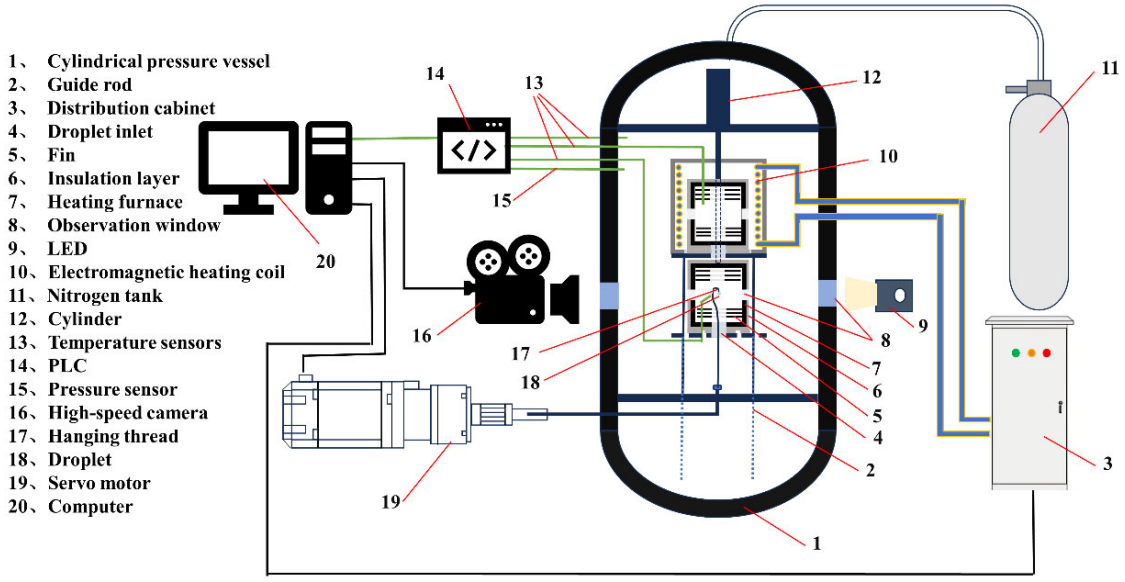

Figure 1. Schematic diagram of a single-droplet evaporation device.

As shown in Figure 1, the pressure environment compartment and the furnace body are mounted with quartz glass windows on opposite sides at the same horizontal linear position for backlight entry and high-speed image recording, respectively. The temperature inside the heating furnace is regulated by a K-type sensor set on the wall of the heating furnace as a feedback signal to start and stop the fast electromagnetic heating device. The outer side of the heating furnace and the outer side of the electromagnetic heating device are equipped with a heat preservation layer made of aluminum silicate to ensure the stability of the temperature inside the furnace.

As shown in Figure 2, the bottom of the heating furnace has a circular hole with a diameter of 28 mm, through which the liquid droplet passes through the heating furnace during its descent to a specified position. On the one hand, the hole at the bottom can prevent the liquid droplets from being preheated in advance during the heating process of the heating furnace, and on the other hand, by controlling the up and down movement of the heating furnace, the falling of the liquid droplets off the wire during movement can be avoided. By adjusting the cylinder pressure, it can be ensured that the time interval between starting and running the heating furnace to the specified position is within 0.3 s.

Figure 2. Photograph of the high-temperature evaporation furnace.

2.2. Data Processing Methods

The process of droplet evaporation with varying initial diameters was recorded using a camera capable of high-speed capture. Increasing the image resolution can reduce the error in the process of extracting droplet diameter data from images during the evaporation process. A resolution of 1024 × 1024 pixels and a speed of 200 fps were selected to record all the experimental images for this paper. The distributions of the initial diameters of large-diameter droplets (D_L), medium-diameter droplets (D_M), and small-diameter droplets (D_S) at different pressures, together with the mean and standard deviation, are shown in Figure 3.

By analyzing the diameter changes during the evaporation of droplets with different initial diameters, the evaporation characteristics of droplets with different initial diameters under different working conditions can be obtained. Based on a previous study [29], the method of calculating the equivalent diameter of a droplet by projecting the area was chosen as the processing method for the relevant images in this paper. Figure 4 shows a schematic diagram of the Python-based image processing program. First, a region of interest (ROI, 150 × 150 pixels) was selected from the image, which could completely describe the changes in the droplets during the evaporation process. Second, the Otsu method was chosen to remove the background around the droplet from the 8-bit grayscale image to obtain an 8-bit black-and-white (B/W) image; again, the morphological image processing (erosion first, then dilation) was applied to the white cavity in the middle of the droplet; and finally, a metal wire with a diameter of 1 mm was used to calibrate the physical resolution of the image (32 pixels/mm), and the number of pixels in the droplet area (the black pixel dots) was counted to obtain the projected area. At the end of droplet evaporation, the projected area occupied by the hanging wire was determined and subtracted from all images to obtain the equivalent projected area of the droplet and to determine the equivalent circle diameter.

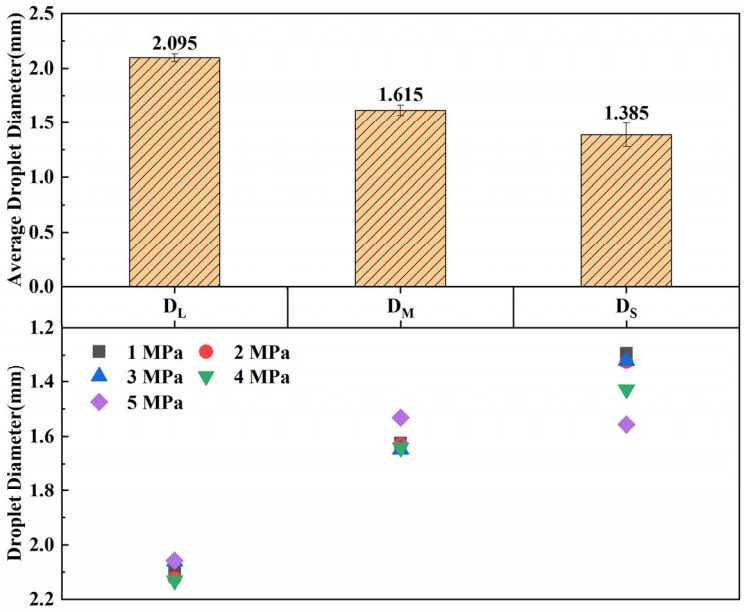

Figure 3. Distribution of different initial droplet diameters with mean diameter and standard deviation.

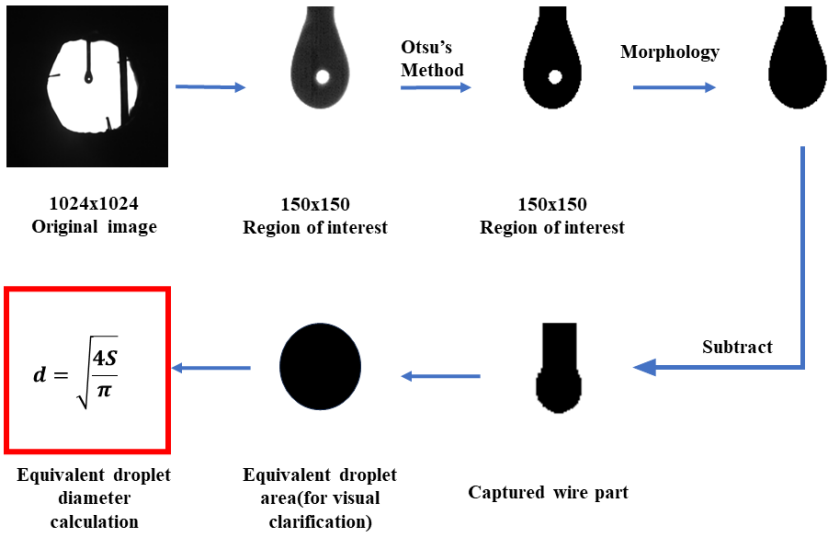

Figure 4. Schematic diagram of the image processing program.

There are usually two reasons for errors in droplet diameter, one being the physical resolution during image calibration. The other is the optical effect in high-temperature and high-pressure environments. In this paper, the experimental temperature was 473 K, the pressure was 1–5 MPa; and the temperature and pressure were relatively low, so we only focused on the error caused by the physical resolution. If the error in the image calibration process is ±1 pixel point, for example, for a droplet (d_0 = 2.0988 mm) at an ambient pressure of 1 MPa, the corresponding error is 3.1%, and if the error in the image calibration process is −1 pixel point, the corresponding error is 3.2%. The distribution of the different initial droplet diameters and the mean and standard deviation results obtained are shown in Figure 3.

3. Results and Discussion

3.1. Evaporation Properties of Liquid Droplets

Figures 5–7 show a series of images of the evaporation processes of large-diameter droplets, medium-diameter droplets, and small-diameter droplets at an ambient tempera-

ture of 473 K and different ambient pressures. As shown in Figures 5–7, the evaporation process of the UDMH droplets under different ambient pressures is composed of two stages. In the first stage, the droplet diameter does not change significantly; at this time, the droplet is in a warming process. In the second stage, the diameter of the droplet significantly decreases with time under all working conditions. Droplets are heated to until the droplet is completely evaporated, and the corresponding image shows only the hanging wire. With increasing pressure, the time to the complete evaporation of the droplet gradually decreases; for the same droplet diameter, an increase in the pressure does not produce a more obvious effect on the thermal conductivity of the ambient gas coefficient, which significantly enhances the role of the thermal conductivity.

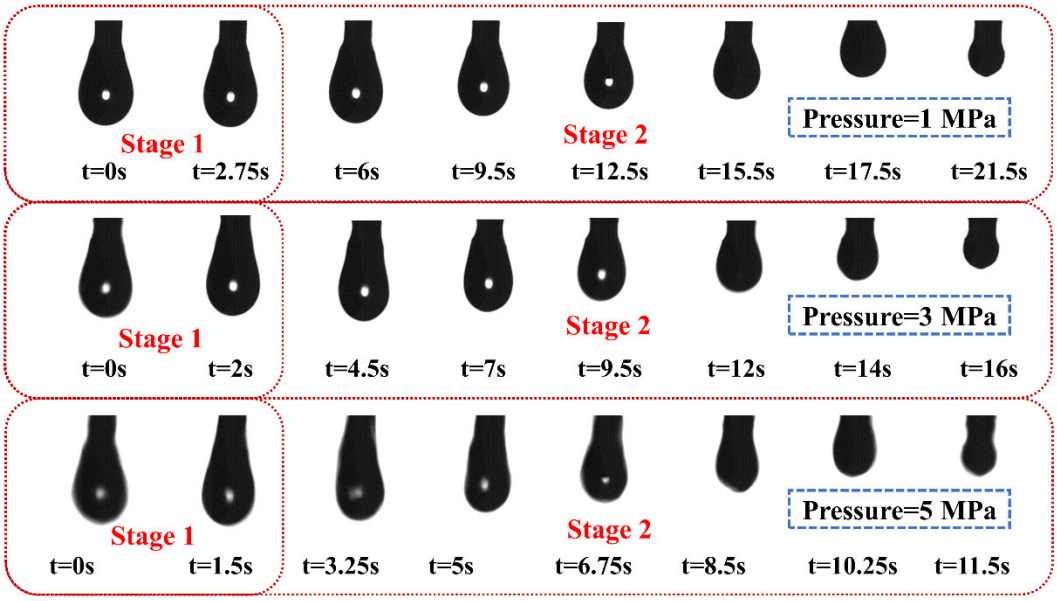

Figure 5. Evaporation images of large-diameter droplets at different pressures at 473 K.

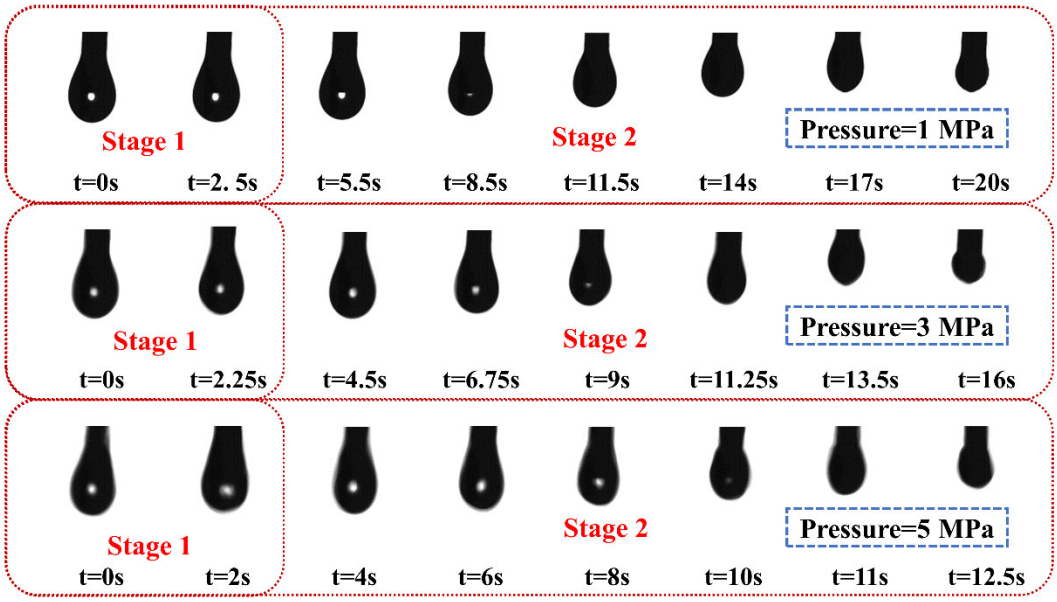

Figure 6. Evaporation images of medium-diameter droplets at different pressures at 473 K.

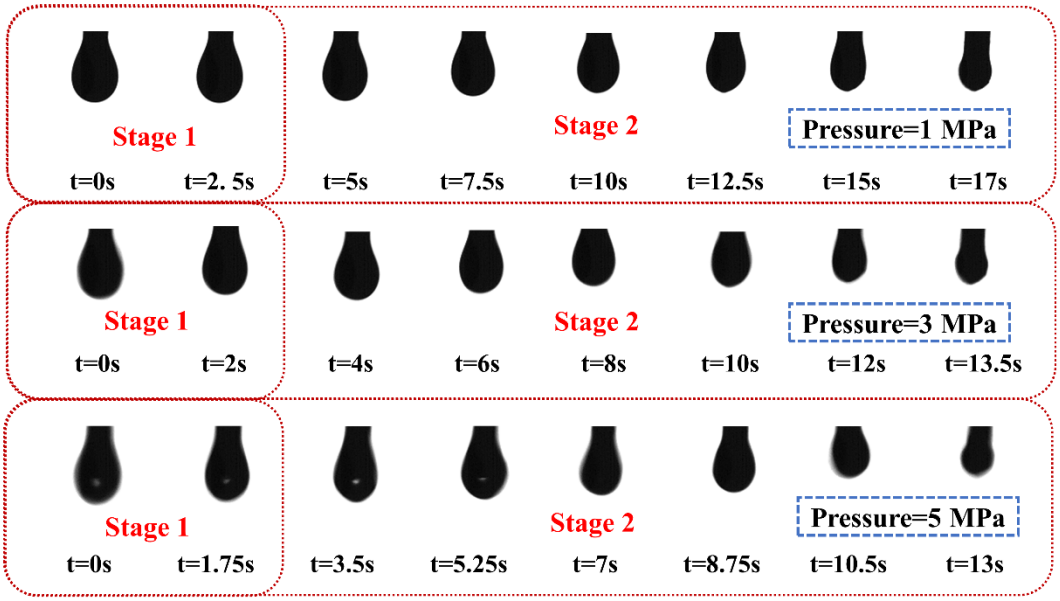

Figure 7. Evaporation images of small-diameter droplets at different pressures at 473 K.

Figure 8a–e show the variation process of the squared droplet diameter of droplets with different initial diameters over time at the same ambient temperature (473 K) and different ambient pressures (1–5 MPa). Since it is difficult to generate droplets with identical initial diameters during the experiments, the squared droplet diameters and droplet evaporation lifetimes were normalized to evaluate the evaporation characteristics of the UDMH droplets with different initial diameters in subcritical environments. An example of the evaporation process of large-diameter UDMH droplets is given in Figure 8f, which shows the variation in the square of the diameter of a large-diameter UDMH droplet with normalized time. The curve shows two completely different variations in squared droplet diameter during the evaporation of a large-diameter UDMH droplet. During the initial phase of UDMH droplet evaporation, as the temperature increases, the droplet density decreases, causing it to expand. At the same time, mass diffusion during evaporation leads to a decrease in the droplet diameter, and a dynamic equilibrium is reached between the two. This change as the droplet undergoes heating is referred to as the transient heating phase. Throughout this heating process, the sensible heat of the droplet gradually increases until it reaches the "wet bulb temperature". During the transient heating phase, the diameter of the droplet clearly changes. The droplet diameter begins to decrease, and the dominant factor causing this decrease is the evaporation process. The decrease in the droplet diameter follows the d^2 law. This phase is defined as the steady-state evaporation phase of the droplet. For the results shown in Figure 8f, the maximum increment in the squared droplet diameter is approximately 1.36% of the square of the initial diameter of the droplet, which corresponds to 0.68% of the diameter.

The definitions of the transient heating time ($\Delta\tau_{h1}$), droplet evaporation lifetime ($\Delta\tau_{lt}$), steady-state evaporation time ($\Delta\tau_{h2}$), and evaporation rate (K_{ave}) are given in Figure 8f. For the calculation of the evaporation rate, the absolute value of the slope of the curve obtained by fitting the data points between $d^2/d_0^2 = 0.8$ and $d^2/d_0^2 = 0.1$ and their corresponding normalized times using the least-squares method is the evaporation rate of the droplet, and the evaporation lifetime of the droplet is defined as the normalized time that corresponds to the intersection of the fitted curve and the abscissa. The transient heating time is defined as the normalized time of the fitted curve at $d^2/d_0^2 = 1$; the steady-state evaporation time is defined as the normalized time remaining after subtracting the transient heating time from the droplet evaporation lifetime.

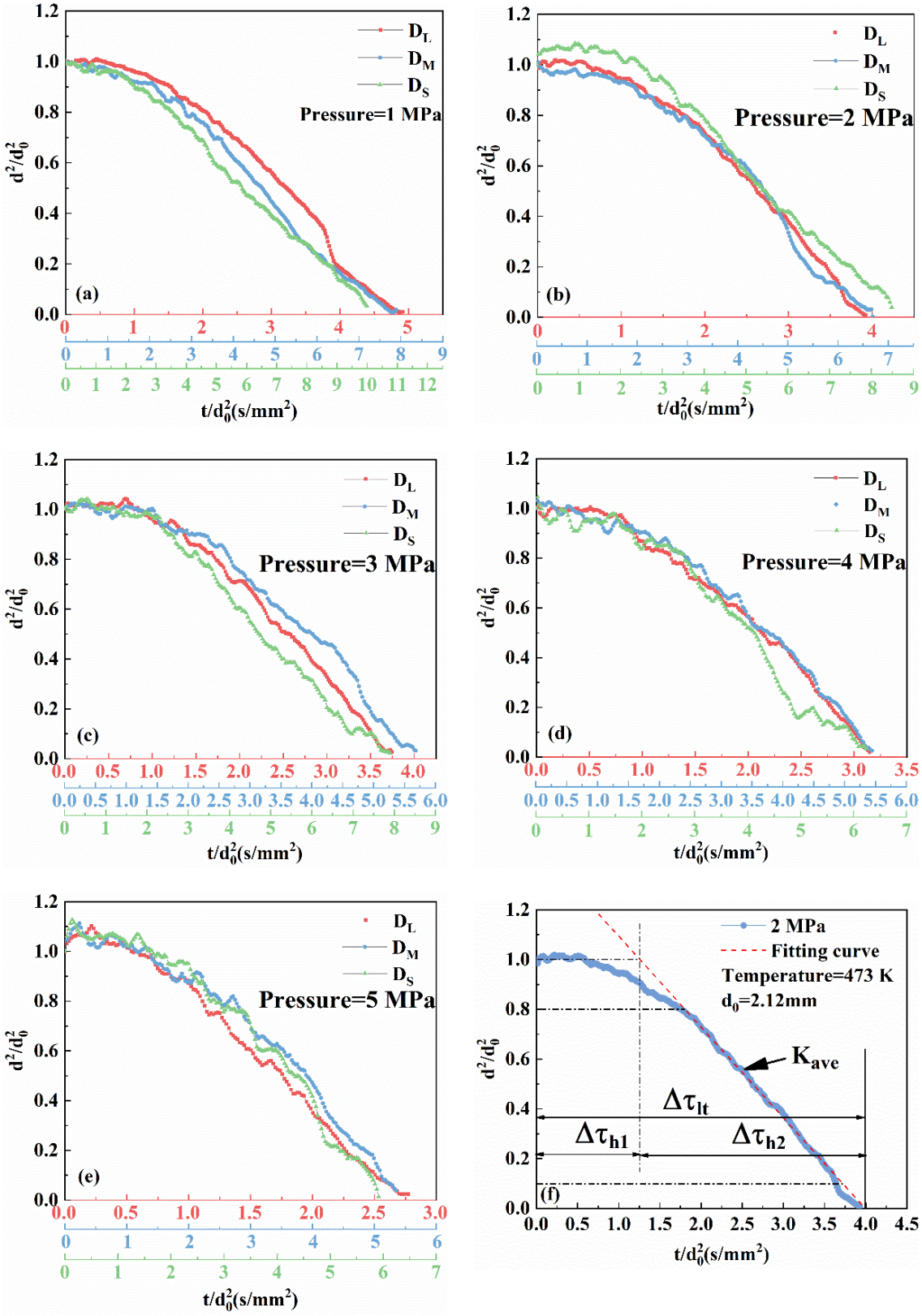

Figure 8. Variations in the squared droplet diameter with time for different initial droplet diameters. (**a**) Pressure = 1 MPa; (**b**) Pressure = 2 MPa; (**c**) Pressure = 3 MPa; (**d**) Pressure = 4 MPa; (**e**) Pressure = 5 MPa; (**f**) Pressure = 2 MPa, Temperature = 473 K.

3.2. Effect of Initial Droplet Diameter on Evaporation Characteristics

Figure 9a–c depict the variations in the evaporation lifetimes of the UDMH droplets with different initial diameters at different ambient pressures. The comparative results of the contribution of the variation in the lifetime of the different evaporation stages to the variation in the evaporation lifetime of the droplet are also shown, using Equation (1) to quantitatively describe the contribution X [30].

$$X = \frac{\Delta\tau_{\mathrm{h\_S}} - \Delta\tau_{h_{M/L}}}{\Delta\tau_{lt\_S} - \Delta\tau_{lt_{M/L}}} \times 100\% \quad (1)$$

where $\Delta\tau_{\mathrm{h\_S}}$ and $\Delta\tau_{h_{M/L}}$ are the normalized times of the same evaporation stage under small-diameter droplets and medium-diameter droplets or large-diameter droplets, respectively, and $\Delta\tau_{lt\_S}$ and $\Delta\tau_{lt_{M/L}}$ are the normalized lifetimes of the small-diameter droplets and medium-diameter droplets or large-diameter droplets, respectively.

Figure 9 shows that at low ambient pressures ($\leq$3 MPa), as the droplet's initial diameter increases, the magnitude of the change in the steady-state evaporation time gradually increases as a proportion of the magnitude of the change in the evaporation lifetime of the droplet, and all the results indicate that this proportion is greater than 85%. When the pressure increases above 3 MPa, the proportion of the transient heating time variation in the medium- and large-diameter UDMH droplets gradually decreases to 36.5% and 54.4%, respectively. This is because the droplet evaporation process is closely related to the wet bulb temperature, and droplet evaporation during the mass transfer process is negatively correlated to the wet bulb temperature. When the pressure increases, the heat and mass transfer of the UDMH droplet gradually increase, corresponding to a decrease in the droplet wet bulb temperature. The time required for the droplet temperature to reach the wet bulb temperature will be shorter. Additionally, this process can be analyzed in conjunction with the Rayleigh number shown in Equation (2).

$$R_a = G_r \times P_r = \frac{g\beta L^3 \Delta T}{\nu\alpha} \quad (2)$$

where ν is the kinematic viscosity, α is the thermal diffusion coefficient, β is the gravitational acceleration, L is the characteristic scale, and ΔT is the temperature difference. According to the Rayleigh number shown in Equation (2), the Rayleigh number strongly depends on the characteristic length, and the droplet diameter strongly influences the temperature difference between the surface and the interior of the droplet during the transient heating phase. A droplet with a larger initial diameter tends to experience more intense natural convection inside the droplet, the droplet reaches the wet bulb temperature more quickly, and the magnitude of the change in the transient heating time for a large-diameter droplet under the same ambient conditions is much larger.

This indicates that for medium- and large-diameter droplets under subcritical conditions, the change in the steady-state evaporation time still plays a crucial role in the change in the droplet evaporation lifetime. The importance of the transient heating time gradually increases with increasing pressure, and the contribution of the transient evaporation time for medium-diameter droplets even exceeds that of the steady-state evaporation time.

A more comprehensive study of the factors influencing the droplet evaporation process is needed. We also chose another method for calculation as a supplement, as shown in Equation (3):

$$Y = \frac{\Delta\tau_{h\_S/M/L}}{\Delta\tau_{lt_S/M/L}} \times 100\% \quad (3)$$

where $\Delta\tau_{h\_S/M/L}$ is the normalized time corresponding to the different evaporation stages for droplets with different initial diameters and $\Delta\tau_{lt_S/M/L}$ is the normalized lifetime for droplets with different initial diameters. The results obtained with Equation (3) are shown in Figure 10, which shows that for droplets with different initial diameters, the heat transfer capacity of the ambient gas increases with increasing ambient pressure, which causes the

evaporation lifetime of the droplets to decrease gradually. With increasing pressure, the proportions of the transient heating stage and steady-state evaporation stage during the evaporation lifetime of the droplet fluctuate less, the changes in the corresponding times of the different stages are synchronous, the difference in the effects of the pressure increase on the two stages is small, and with the gradual increase in the initial droplet diameter, the proportions of the different stages in the evaporation lifetime of the droplet are more stable. This is because the influence of the hanging wire on the droplet evaporation process gradually decreases with increasing initial droplet diameter.

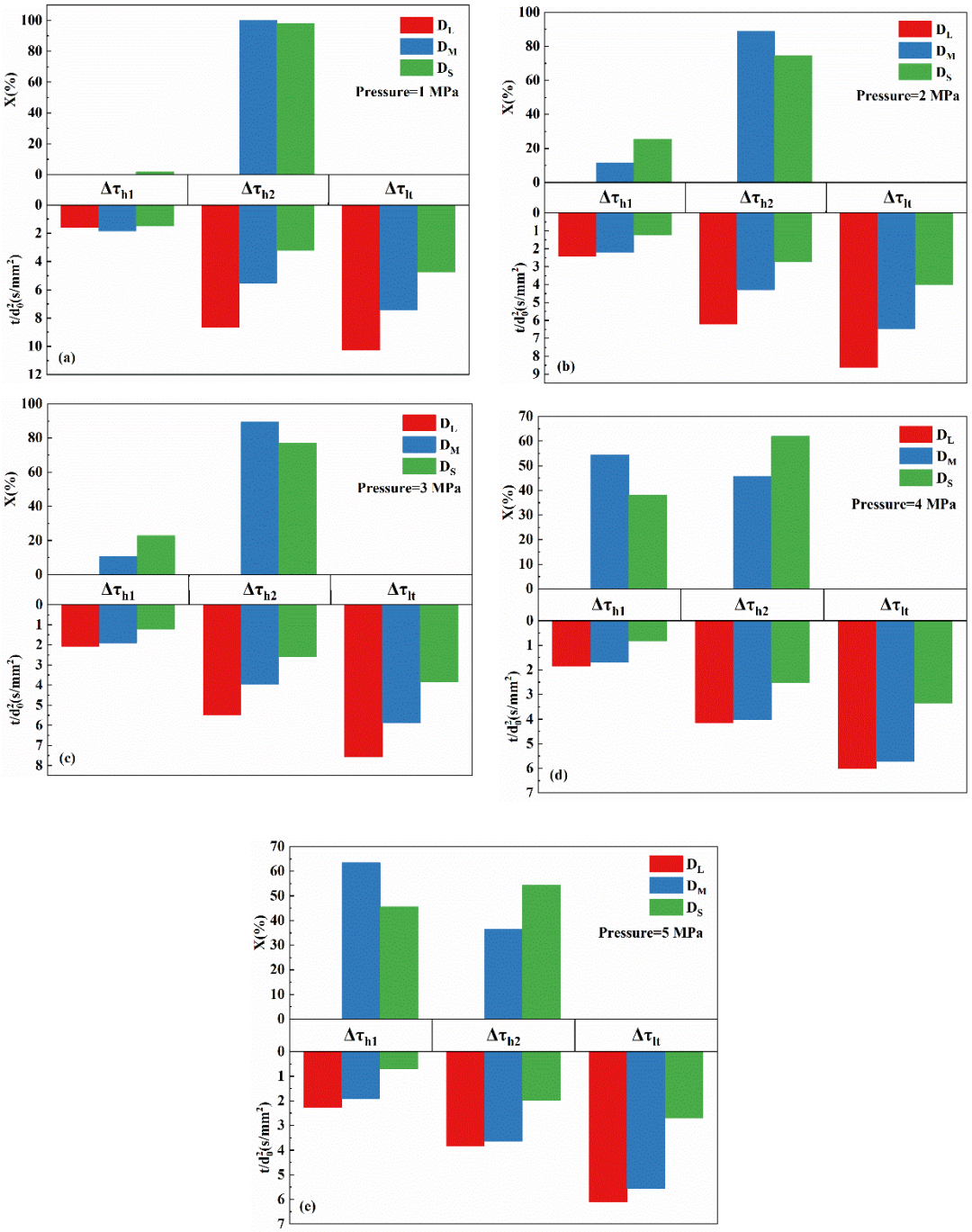

Figure 9. Effect of different evaporation stages on the evaporation lifetime at different pressures. (**a**) Pressure = 1 MPa; (**b**) Pressure = 2 MPa; (**c**) Pressure = 3 MPa; (**d**) Pressure = 4 MPa; (**e**) Pressure = 5 MPa.

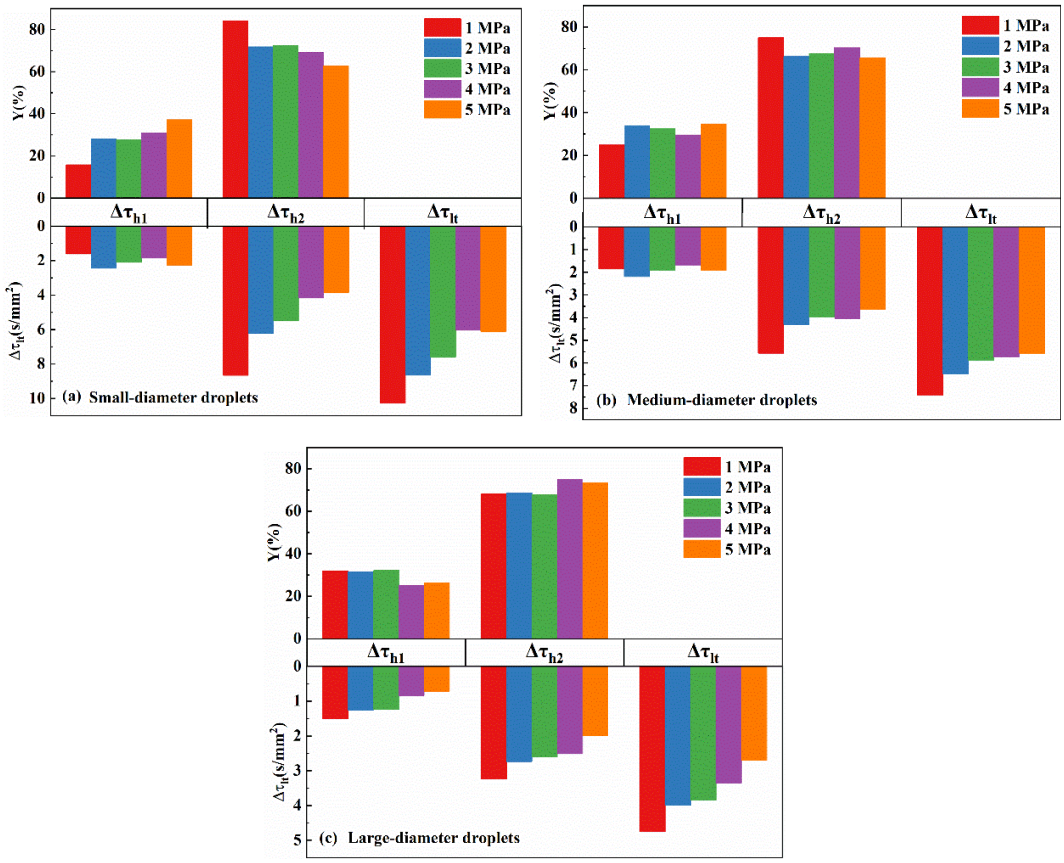

Figure 10. Proportion of different evaporation stages of the evaporation lifetime at different pressures. (**a**) small-diameter droplets; (**b**) medium-diameter droplets; (**c**) large-diameter droplets.

The relative importance of the droplet diameters can be assessed by calculating the percentage reduction in K_{ave} between different initial droplet diameters through Equation (4):

$$\lambda = \frac{K_{ave\_L} - K_{ave_{M/S}}}{K_{ave\_L}} \times 100\% \quad (4)$$

where K_{ave_L} is the evaporation rate of large-diameter droplets and $K_{ave_{M/S}}$ is the evaporation rate of medium- and small-diameter droplets. Figure 11 shows the dependence of the evaporation rate constant on the initial droplet diameter under subcritical conditions. The figure demonstrates that the rate of evaporation of the droplet decreases progressively as the initial droplet diameter decreases under all experimental conditions. In particular, the difference in the evaporation rate between the medium- and small-diameter droplets decreases rapidly when the ambient pressure increases to 4 MPa and 5 MPa. From the initial droplet diameter distributions in Figure 3, it can be inferred that this is due to the gradual narrowing of the difference between the sizes of the medium-diameter droplets and the small-diameter droplets at 4 MPa and 5 MPa. At low ambient pressures ($\leq$3 MPa), the percentage of narrowing of the difference between the sizes of the droplets reached $38 \pm 4\%$ and $52 \pm 6\%$ for the medium-diameter and small-diameter droplets, respectively. When the pressure was increased to 4 MPa and 5 MPa, the proportional difference between them narrowed rapidly. Combined with the initial droplet diameter distribution, it can be concluded that when the droplets are in a subcritical environment, the change in the initial droplet diameter may still have a large effect on the droplets below a small diameter.

The relationship between the decrease in the evaporation rate and the initial droplet diameter can be examined together with the Rayleigh number (Equation (3)). When a droplet enters a high-temperature environment, the temperature on the surface of the droplet increases

rapidly, a temperature gradient occurs in the interior of the droplet, the density distribution inside the droplet changes, and the resulting convection process affects the heat transfer of the droplet. Because of the strong dependence of the Rayleigh number on the characteristic length and the large temperature variations at the droplet surface, droplets with larger initial diameters tend to experience more intense natural convection inside the droplet.

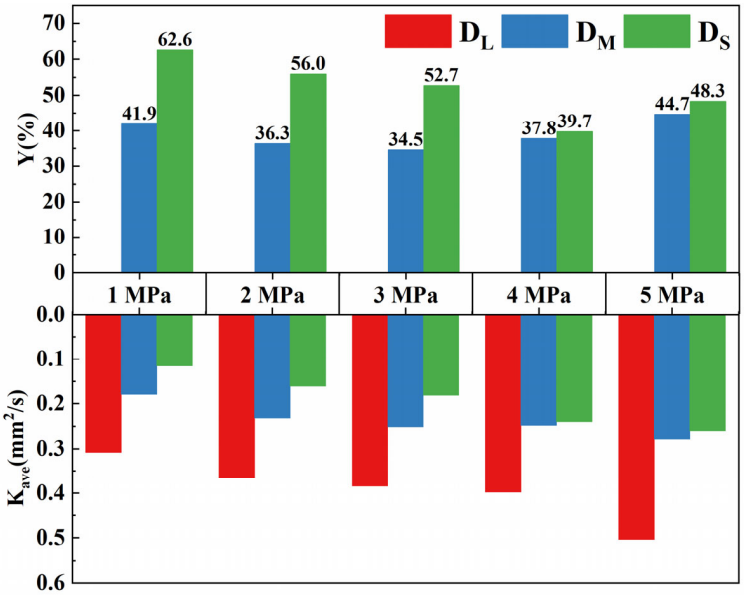

Figure 11. Effect of the initial droplet diameter on the evaporation rate at different ambient pressures.

Figure 12 shows the dependence of the droplet evaporation lifetime on the initial droplet diameter at different ambient pressures. As shown in the figure, the droplet evaporation lifetime gradually increases with decreasing initial droplet diameter under all pressure conditions. This is because the temperature difference between the inside and outside of the small-diameter droplet is lower than that between the inside and outside of the large-diameter droplet, which results in the intensity of the natural convection inside the large-diameter droplet being stronger than that inside the small-diameter droplet.

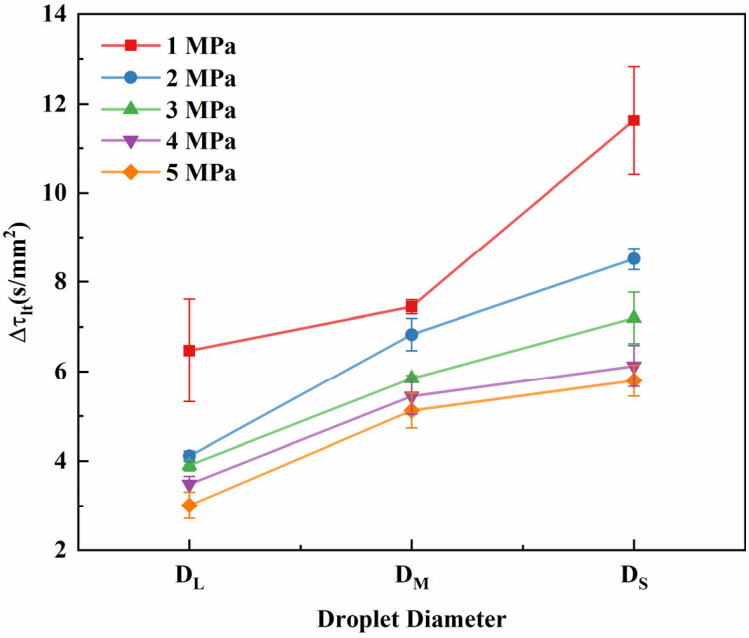

Figure 12. Effect of initial droplet diameter on droplet evaporation lifetime.

4. Conclusions

In this paper, the evaporation characteristics of UDMH droplets with different initial diameters under different operating conditions (temperature = 473 K, pressure = 1–5 MPa) are experimentally investigated and analyzed, and the following conclusions are obtained:

(1) The evaporation processes of UDMH droplets with different initial diameters in a subcritical environment have the same general pattern. All of the droplets undergo a short transient heating phase and a steady-state evaporation phase obeying d^2. In particular, the expansion of the steady-state evaporation phase gradually increases with increasing ambient pressure. The change in diameter squared $\left(\Delta d^2\right)_{max}$ increases from 1.03% at 1 MPa to 12.48% at 5 MPa.

(2) When droplets of different initial diameters are placed in subcritical environments, the evaporation rate decreases linearly with decreasing droplet diameter, and the evaporation lifetime of the droplets increases linearly. Changes in the initial droplet diameter may still have a large effect on droplets smaller than the small-diameter droplets studied here.

(3) When the ambient pressure is not greater than 3 MPa, the change in the steady-state evaporation time accounts for more than 70% of the change in the droplet evaporation lifetime for both medium- and large-diameter droplets compared to small-diameter droplets. The change in the steady-state evaporation time plays a crucial role in the change in the droplet evaporation lifetime. With increasing pressure, the proportion of the variation in the transient heating time to the variation in the droplet evaporation lifetime gradually increases to more than 45%. The change in the transient heating time for medium-diameter droplets is more important than that for large-diameter droplets in terms of the droplet evaporation lifetime.

Author Contributions: Conceptualization, G.W. and W.N.; methodology, G.W.; software, G.W.; validation, H.W., G.W. and C.Y.; formal analysis, C.Y. and G.W.; investigation, S.Z. and C.Y.; resources, W.N. and H.W.; data curation, G.W.; writing—original draft preparation, G.W.; writing—review and editing, G.W., W.N. and H.W.; visualization, G.W. and C.Y.; supervision, S.Z.; project administration, W.N. and H.W.; funding acquisition, W.N. All authors have read and agreed to the published version of the manuscript.

Funding: This work was supported by the National Natural Science Foundation of China (Grant No. 12102482) and the Beijing Natural Science Foundation (No. 3222062).

Data Availability Statement: The data that support the findings of this study are available from the corresponding author upon reasonable request.

Conflicts of Interest: The authors declare no conflicts of interest.

References

1. Sánchez, A.L.; Urzay, J.; Liñán, A. The role of separation of scales in the description of spray combustion. *Proc. Combust. Inst.* **2015**, *35*, 1549–1577. [CrossRef]
2. Chigier, N.A. The atomization and burning of liquid fuel sprays. *Prog. Energy Combust. Sci.* **1976**, *2*, 97–114. [CrossRef]
3. Fei, L.; Qin, F.; Wang, G.; Luo, K.H.; Derome, D.; Carmeliet, J. Droplet evaporation in finite-size systems: Theoretical analysis and mesoscopic modeling. *Phys. Rev. E* **2022**, *105*, 025101. [CrossRef] [PubMed]
4. Yin, J.; Chen, S.-Y.; Zhu, D.-Q.; Xue, S.-Q.; Li, S.-Y.; Zhou, Z.-F.; Liu, B. Experimental investigation on evaporation characteristics of RP-3 aviation kerosene droplet above the critical temperature under various pressure conditions. *Aerosp. Sci. Technol.* **2023**, *140*, 108463. [CrossRef]
5. Huang, J.; Zhang, H.; He, Y.; Zhu, Y.; Wang, Z. Evaporation, Autoignition and Micro-Explosion Characteristics of RP-3 Kerosene Droplets under Sub-Atmospheric Pressure and Elevated Temperature. *Energies* **2022**, *15*, 7172. [CrossRef]
6. Katre, P.; Balusamy, S.; Banerjee, S.; Chandrala, L.D.; Sahu, K.C. Evaporation Dynamics of a Sessile Droplet of Binary Mixture Laden with Nanoparticles. *Langmuir ACS J. Surf. Colloids* **2021**, *37*, 6311–6321. [CrossRef] [PubMed]
7. Xiao, G.; Luo, K.H.; Ma, X.; Shuai, S. A molecular dynamics study of fuel droplet evaporation in sub- and supercritical conditions. *Proc. Combust. Inst.* **2019**, *37*, 3219–3227. [CrossRef]
8. Strizhak, P.A.; Volkov, R.; Misyura, S.Y.; Lezhnin, S.; Morozov, V.S. The role of convection in gas and liquid phases at droplet evaporation. *Int. J. Therm. Sci.* **2018**, *134*, 421–439. [CrossRef]
9. Fan, D.; Wang, H.; Cui, C.; Wang, Y. Predictive simulation of evaporation and diffusion pattern of unsymmetrical dimethylhydrazine in natural environment. *Comput. Simul.* **2017**, *34*, 6. [CrossRef]

10. Huang, Z.; Chen, X.; Ping, Y.; Wang, X. Evaporation Characteristic of Unsymmetrical Dimethylhydrazine Propellant in Storage. *Missiles Space Veh.* **2011**, *30*, 58–61. [CrossRef]
11. Huang, Z.; Luo, F.; Shi, H. Numerical Simulation of Diffusion of Unsymmetrical Dimethylhrazine Under Storage Condition. *Sci. Technol. Rev.* **2011**, *29*, 67–70. [CrossRef]
12. Yin, T. Experimental study on the droplet evaporation process and influence factors. In Proceedings of the AIAA 2014-3570, 50th AIAA/ASME/SAE/ASEE Joint Propulsion Conference, Cleveland, OH, USA, 28–30 July 2014.
13. Faeth, G.M. Mixing, transport and combustion in sprays. *Prog. Energy Combust. Sci.* **1987**, *13*, 293–345. [CrossRef]
14. Szekely, G.A.; Faeth, G.M. Effects of envelope flames on drop gasification rates in turbulent diffusion flames. *Combust. Flame* **1983**, *49*, 255–259. [CrossRef]
15. Ju, D.; Zhang, T.; Xiao, J.; Qiao, X.; Huang, Z. Effect of droplet sizes on evaporation of a bi-component droplet at DME (dimethyl ether)/n-heptane-fueled engine conditions. *Energy* **2015**, *86*, 257–266. [CrossRef]
16. Brenn, G.; Deviprasath, L.J.; Durst, F.; Fink, C. Evaporation of acoustically levitated multi-component liquid droplets. *Int. J. Heat Mass Transf.* **2007**, *50*, 5073–5086. [CrossRef]
17. Abramzon, B.; Sirignano, W.A. Droplet vaporization model for spray combustion calculations. In Proceedings of the 26th Aerospace Sciences Meeting, Reno, NV, USA, 11–14 January 1988.
18. Miller, R.S.; Harstad, K.G.; Bellan, J. Evaluation of equilibrium and non-equilibrium evaporation models for many-droplet gas-liquid flow simulations. *Int. J. Multiph. Flow* **1998**, *24*, 1025–1055. [CrossRef]
19. Verwey, C.; Birouk, M. Experimental investigation of the effect of natural convection on the evaporation characteristics of small fuel droplets at moderately elevated temperature and pressure. *Int. J. Heat Mass Transf.* **2018**, *118*, 1046–1055. [CrossRef]
20. Dgheim, J.; Abdallah, M.; Nasr, N.B. Enhanced Evaporation of Droplet of Ternary Component Under the Effect of Thermo-physical and Transport Properties Variability. *Arab. J. Sci. Eng.* **2018**, *43*, 2181–2194. [CrossRef]
21. Liu, L.; Bi, Q.-C.; Liu, W.-M.; Qi, F.-C.; Bi, X.-G. Experimental and Theoretical Investigation on Rapid Evaporation of Ethanol Droplets and Kerosene Droplets During Depressurization. *Microgravity Sci. Technol.* **2011**, *23*, 89–97. [CrossRef]
22. Liu, L.; Liu, Y.F.; Mi, M.; Wang, Z.; Jiang, L. Evaporation of a bicomponent droplet during depressurization. *Int. J. Heat Mass Transf.* **2016**, *100*, 615–626. [CrossRef]
23. Lorenzini, G.; Conti, A.; De Wrachien, D. Computational Fluid Dynamics (CFD) Picture of Water Droplet Evaporation in Air. *Irrig. Drain. Syst. Eng.* **2012**, *1*, 1000101. [CrossRef]
24. Ruan, Y.; Chen, L.; Liu, X.; Chen, S.; Hou, Y. Numerical Study of Evaporation and Motion Characteristics of Liquid Nitrogen Droplet in High-Speed Gas Flow. *IOP Conf. Ser. Mater. Sci. Eng.* **2017**, *278*, 012130. [CrossRef]
25. Stagni, A.; Calabria, R.; Frassoldati, A.; Cuoci, A.; Faravelli, T.; Chiariello, F.; Massoli, P. Kinetic Modeling of the Ignition of Droplets of Fast Pyrolysis Bio-oil: Effect of Initial Diameter and Fuel Composition. *Ind. Eng. Chem. Res.* **2021**, *60*, 6719–6729. [CrossRef] [PubMed]
26. Verwey, C. An Experimental Investigation of the Effect of Fuel Droplet Size on the Vaporization Process in a Turbulent Environment at Elevated Temperature and Pressure. Master's Thesis, University of Manitoba, Winnipeg, MB, Canada, 2017.
27. Verwey, C.; Birouk, M. Experimental investigation of the effect of droplet size on the vaporization process in ambient turbulence. *Combust. Flame* **2017**, *182*, 288–297. [CrossRef]
28. Birouk, M.; Toth, S.L. Vaporization and Combustion of a Soybean Biodiesel Droplet in Turbulent Environment at Elevated Ambient Pressure. *Combust. Sci. Technol.* **2015**, *187*, 937–952. [CrossRef]
29. Wu, G.; Wang, Z.; Yang, C.; Wang, H.; Nie, W. Experimental study of the evaporation characteristics of unsymmetrical dimethylhydrazine in a sub-supercritical environment. *Phys. Fluids* **2024**, *36*, 023321. [CrossRef]
30. Han, K.; Zhao, C.L.; Fu, G.; Zhang, F.J.; Pang, S.P.; Li, Y.C. Evaporation characteristics of dual component droplet of benzyl azides-hexadecane mixtures at elevated temperatures. *Fuel* **2015**, *157*, 270–278. [CrossRef]